

# 10



# Feasibility of monitoring cold fronts of geothermal doublets using 4D active electromagnetic techniques – a field trial in the Dogger play in the Paris Basin

F. Dubois, A. Stopin, F. Bretaudeau and P. Wawrzyniak

---

This project aimed to develop a methodology for imaging the “cold fronts” using the surface-to-borehole Controlled Source Electromagnetic Method (CSEM). To achieve this goal, a CSEM data acquisition campaign was being carried out on an operational geothermal doublet, using a surface-to-borehole measurement configuration. The downhole measurement tool (an induction

magnetic field sensor) developed by the LBNL (Lawrence Berkeley National Laboratory of the University of California), and the detectability of the “cold fronts” had to be validated in situ. The doublet where the measurements were taken is part of Dalkia’s geothermal plant in Evry. In early January 2022, a series of injection points, laid out according to the recommendations from different modellings were prepared in anticipation of the acquisition campaign. On the 1st of March, SDP logging team lowered the probe into the well but was unable to pass through the open-hole section. After some adjustments, the probe successfully detected the surface source signal. Data analysis confirmed that the observed signal was indeed emitted by the surface source, thus validating a key aspect of the technology. Additionally, the models indicated that the secondary field generated by a cold front exceeds the noise level recorded by the downhole probe, demonstrating the detectability of the cold front.

## Introduction

This project is initiated as part of the Géodénergies program. Its goal is to develop a methodology for detecting and monitoring the cold front progress between geothermal doublets of the Dogger formation using Controlled Source Electromagnetic (CSEM) methods. From a theoretical standpoint, the cold-water plume is associated with a variation in electrical resistivity within the reservoir (Revil et al., 1998), which can be detected by geophysical CSEM methods (Wawrzyniak et al., 2016). The project consists of two main parts:

1. At the laboratory scale, a calibration of resistivity variations as a function of temperature and frequency specific to the Dogger formation is conducted to accurately characterize this relationship.
2. Then, at the reservoir scale, a CSEM measurement campaign is carried out on a geothermal doublet using a surface-to-borehole measurement configuration. For this, a magnetic probe developed by LBNL (Lawrence Berkeley National Laboratory at the University of California) is lowered into the production well of the Dogger doublet. This will allow for in situ demonstration of the detectability of the “cold front”. The Evry geothermal doublet operated by Dalkia.

In this study case, we will introduce motivations and a summary of the technology used. We then describe the measurement design, including all preparatory work and the campaign’s execution. Finally, we address the data processing and the interpretation of the results, leading to the validation of the cold fronts detectability.

## 10.1 Context

The risk of thermal breakthrough is a long-term consequence of operating Dogger geothermal doublets with reinjection of cooled brine back into the original aquifer. Currently, measuring the temperature at the wellhead of the production well is the only parameter that enables detection of the arrival of the “cold front”. Thermo-hydrodynamic (TH) predictive modeling allows for extrapolation of its dynamic behavior (Figure 10.1) but cannot precisely predict its arrival in time and space. Consequently, cases of thermal breakthrough may occur unexpectedly, as was the case in L’Hay-les-Roses (1 °C decrease after 30 years of operation) and Alfortville (5 °C decrease after 30 years of operation).

At present, there is no tool available for measuring the aquifer temperature other than direct measurement within a well. The proposed technological development is an important element for monitoring geothermal reservoirs.

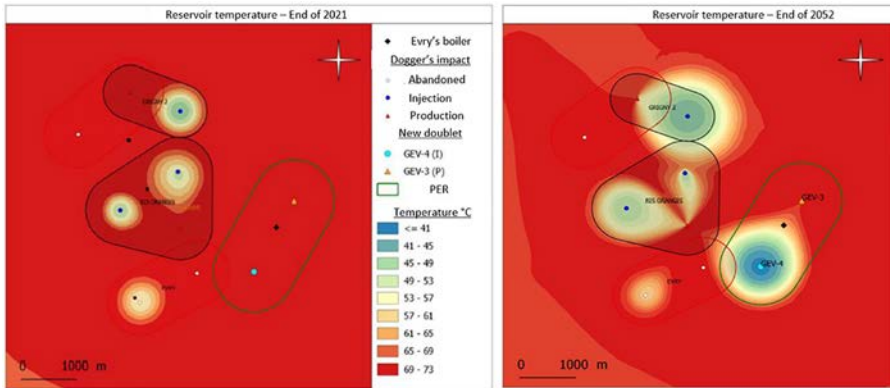


**Figure 10.1** Example of Thermo-Hydrodynamic (TH) modeling used to “predict” the behavior of the cold front over time. Extracted from the activity report submitted by Dalkia for the Evry site.

The CSEM method is sensitive to variations in the subsurface’s electrical resistivity. A source injects electric current into the ground using a square wave signal of predetermined frequency and intensity. One or more receivers simultaneously record electromagnetic fields (electric, magnetic, or both) at the surface or in the borehole. These fields combine the primary field (signal emitted by the source) and a secondary field generated by the distribution of subsurface resistivities. After data processing, the calculated transfer functions can then be “inverted” (a mathematical process) to retrieve the subsurface structure in terms of electrical resistivity.

Wawrzyniak (2019) proposed using CSEM for borehole detection of the cold front within the CO<sub>2</sub> Dissolved project. This work provided guidances and recommendations on the types of sources/receivers and their configurations to use, and it

demonstrated the theoretical detectability of the cold front, particularly identifying the frequencies at which the cold front response would be maximal. We use galvanic sources, injecting current between two electrodes (“poles”) placed in the ground. The placement of these sources is crucial for the success of such measurements. Specifically, it is essential to consider:

1. The distance between the source(s) and receiver(s),
2. The length of the injection dipole(s), or the distance between two electrodes,
3. The orientation of the injection dipole(s),
4. The injected current intensity, related to the grounding resistance (depending on the type of transmitter).

Modeling conducted by Wawrzyniak (2019) and ITES (Strasbourg University) provided guidance on optimal source configurations. For the receivers, preliminary studies showed that a single receiver positioned at the bottom of the well significantly improves the likelihood of capturing the signal. Urban environments have high anthropogenic electromagnetic noise, which can mask the signal. An induction probe is used as the receiver, since measuring the electric field in a cased well must be complex.

## 10.2 Acquisition

The geothermal doublet used for borehole measurements is the Dalkia-operated one in Evry. The injection well GEV4 is targeted, and six zones where injection sites could be established around the well’s shoe have been selected (see Figure 10.2). These sites were surveyed in October 2021. During the survey, factors likely to impact a CSEM survey includes:

1. Presence of power lines, fences, or pipelines.
2. Soil resistivity measurements in areas intended for electrode installation using electrical resistivity tomography (ERT, dipole-dipole) and TDEM with the TEMFAST device (aemr.net). The orientation of the injection dipole(s),
3. Site accessibility.
4. Safety aspects, vehicle traffic, and site activity.

The reconnaissance campaign allowed us to visit each site, resulting in the following observations:

- GEN 1: too small and with high vehicle traffic; low grounding resistance.
- GEN 2: quiet, high electrical resistivity in parts, ample space.
- GEN 3: limited security, low grounding resistance.
- GEN 4: quiet, presence of underground pipes.
- GEN 5: limited security, difficult access, no electrical resistivity measurements.
- GEN 6: inaccessible (fenced), no electrical resistivity measurements.

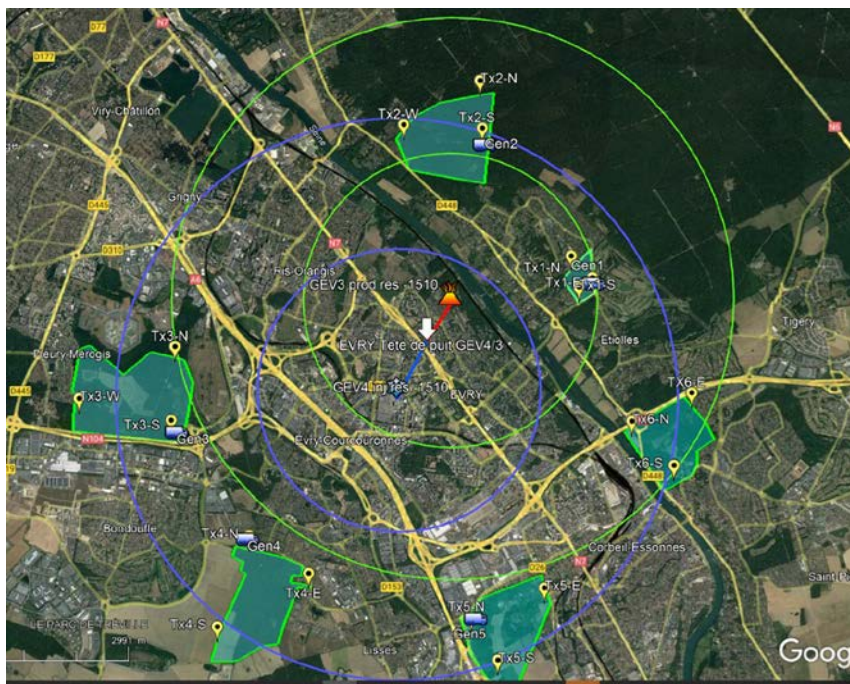


Figure 10.2 Positioning map showing the location of the six identified zones (green polygons) where injection electrodes could be placed. The blue circles are centered on the injection well GEV4, and the green circles on the production well GEV3. The circles have radii of 2 and 4 km.

During a logging control in late October 2021, a foreign object was discovered in the GEV4 injection well. Access to this well was then prohibited due to the increased risk of logging tools becoming stuck. Consequently, the production well GEV3 has been selected by default. Since GEV3 is a production well, access will be more challenging for any future repeat measurements. Furthermore, as the cold front develops in the injection well, it is likely that, even if we gain access to production well in the near future, the cold front signal may be too weak to detect. This will be evaluated during detectability tests, but for this campaign, the decision is to focus on validating the methodology (ability to measure the signal at the bottom of the well and theoretical detectability of the cold front) and to test different source configurations, limiting the campaign to a single injection site. Based on the reconnaissance campaign results, site GEN 2 in the Sénart Forest was selected. Although some surface grounding resistances were high, drilling to a depth of about ten meters should allow for the preparation of electrodes that ensure good current injectivity. Additionally, GEN 2 is the closest site to the well's shoe (2–3 km away) and offers the most suitable conditions in terms of quiet surroundings and adequate space.

In January 2022, a three-day campaign was conducted in the Sénart Forest to drill five holes, each up to 10 meters deep, where copper rods would be placed as injection electrodes. Figure 10.3 shows the location of the drill holes.

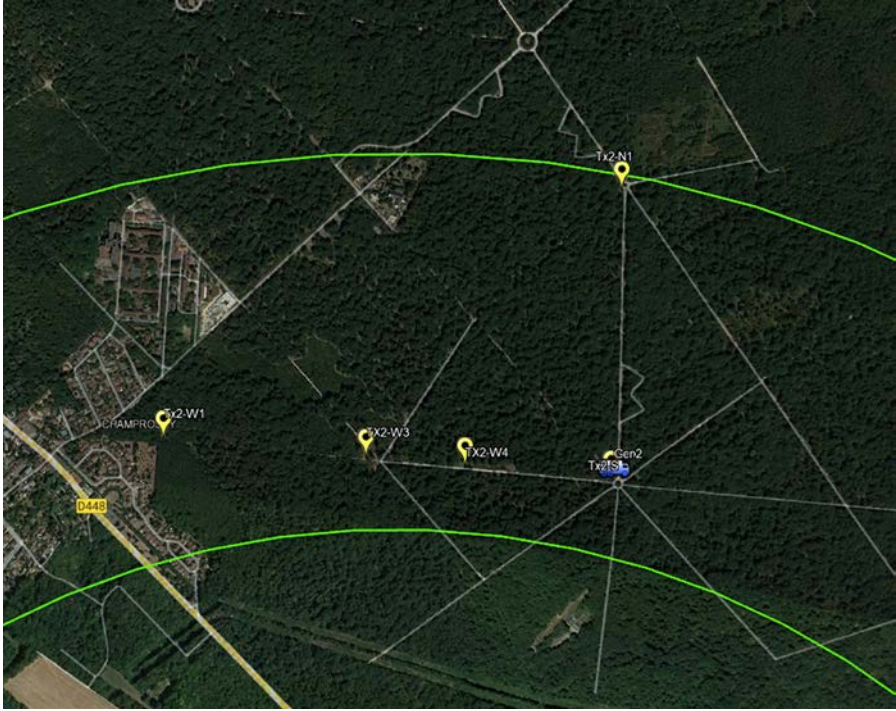


Figure 10.3 Location of the drilled injection electrodes in the Sénart Forest.

We favor the broadside orientation (i.e., perpendicular to the source-to-well shoe axis) of the dipoles, since CSEM modellings indicate this direction to maximize the cold front's response. Then different tests with different dipole lengths in the broadside direction have been conducted as these directly affect the dipole moment of the emitted signal, thus influencing the amplitude of the detectable signal. Finally, a dipole with a radial, in-line orientation is used to validate modeling results showing weaker coupling compared to the broadside orientation.

Between two and five copper rods were inserted into each drilled hole, with bentonite and salt added to enhance coupling between the rods and the ground and lower the grounding resistance. The copper rods were then connected with electrical cable and tape, cut to 10 cm below the surface, and covered with soil, leaves, and stumps to remain inconspicuous and secure. Once the electrodes were prepared, they were connected with electric cables, and grounding resistance was measured to check the dipole's quality and current injection capacity. With

the voltage-regulated transmitter, lower grounding resistance allows for higher injected current. A strong current induces stronger primary and secondary fields, making the signal more detectable. The measured resistances for the four dipoles were as follows:

1. TX2-S – TX2-W1: resistance 50  $\Omega$ ·m, length 1180 m,
2. TX2-S – TX2-W3: resistance 50  $\Omega$ ·m, length 610 m,
3. TX2-S – TX2-W4: resistance 50  $\Omega$ ·m, length 360 m,
4. TX2-S – TX2-N1: resistance 26  $\Omega$ ·m, length 730 m.

These grounding resistances are acceptable and would allow for a minimum current injection of around 10 A (with 550 V voltage). A follow-up inspection in February 2022 confirmed that the electrodes remained intact and well concealed under the branches and leaves placed over them.

### 10.3 Receiver conception

The receiver used to measure the magnetic field at the bottom of the well was developed by LBNL (US) and loaned to BRGM for one year. It is an induction probe (BF4) housed in a fiberglass and epoxy protective casing (see Figure 10.4, left). The BF4 probe is connected to an electronic circuit that provides power and amplifies the measured signal. The probe measures 2.4 meters in length and weighs approximately 20 kg. Its pressure resistance was tested by BRGM at the SDP logging company's logistics base. This test indicated that the probe remained watertight (no internal pressure increase) at a pressure of 220 bars, which is sufficient for the maximum depth of about 1700 meters where it will be deployed in the well. A GO7 head provides the electrical power supply to the probe and transmits the signal back to the surface, while also ensuring the attachment of the probe to the logging cable. With the GO7 head used and due to the design of the probe, it is not possible to connect additional logging instruments to measure other physical properties or to precisely determine the probe's position in the borehole during the measurement campaign. Consequently, when the probe is in the borehole, its location can only be determined by the length of the deployed cable, which is not an exact measurement. Weight bars and centralizers were added below the probe to facilitate its descent and ensure proper positioning at the center of the borehole (see Figure 10.4, right).

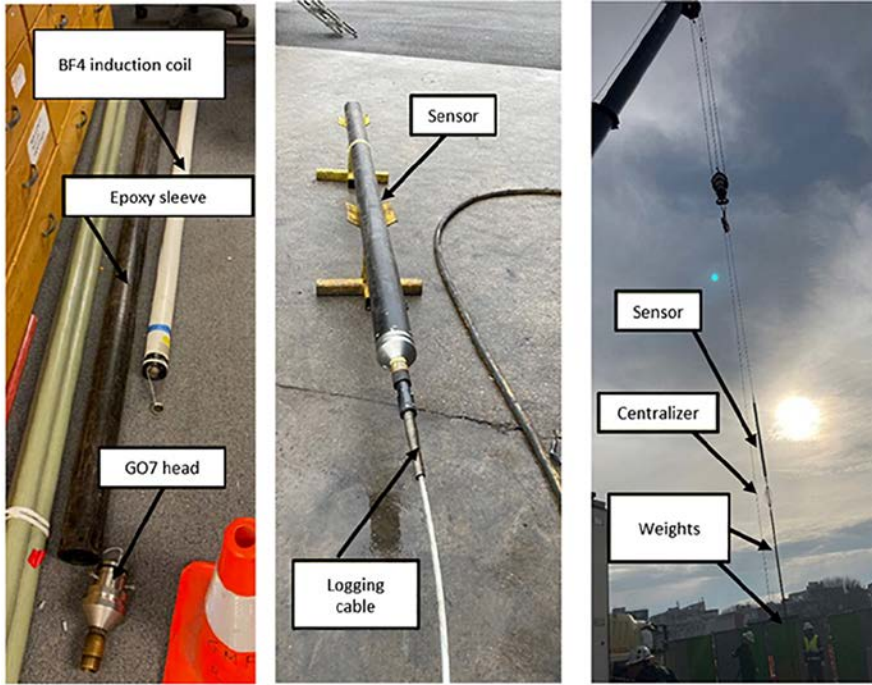


Figure 10.4 Different parts of the LBNL sensors (left) and the probe connected to the logging cable (center), wireline instrument ready to go down into the well (right).

## 10.4 Survey

The survey took place at two sites: the boiler plant site, where the GEV3 borehole (cross-section shown in Figure 10.5) is located and where the logging truck operated the probe (Figure 10.4, right), and the Sénart Forest, where the source (CSEM transmitter) was located. The measurements were carried out on March 1st, 2022, preceded the previous day by the setup of the source equipment and current injection tests to validate proper coupling of the poles. These tests showed improved contact resistance (after pole installation), allowing approximately 15 A of current to be injected. The measurement campaign initially planned to lower the probe into the uncased section of the borehole and perform measurements while raising it, sampling at a minimum of four different depths (Table 10.1). For a given depth, the source emitted the frequency sequence shown in Table 10.2 for a given dipole. This sequence was repeated successively for the four possible dipoles. Once all four dipoles were activated, the probe was raised to the next level, and the operation was repeated.

The schedule planned to start measurements late in the morning (allowing time to install and lower the probe to the bottom of the borehole) and complete measurements for four levels and all dipoles by early evening. The measurements were to be repeated at night to evaluate the signal-to-noise (S/N) ratio, expected to be better at night due to lower anthropogenic noise. However, the transition between cased and uncased sections was complicated to cross. In order to avoid any loss in the well we had to limit our acquisition inside the casing where induced currents may appeared and disturbed the response coming from the reservoir.

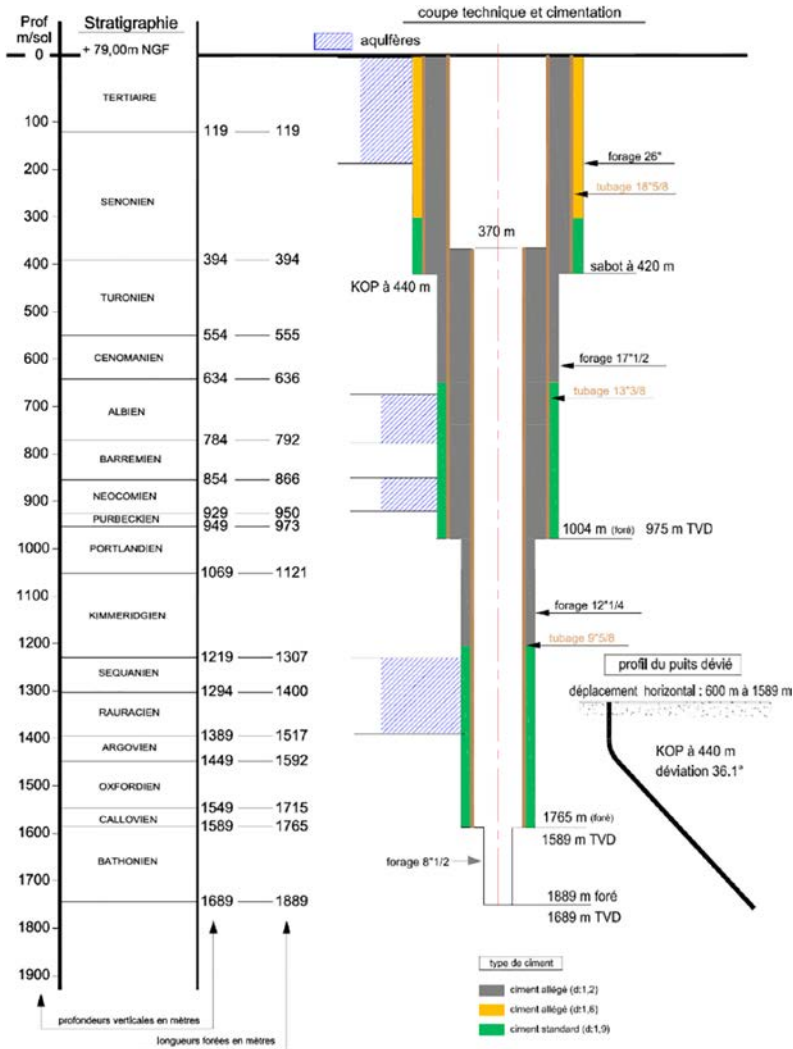


Figure 10.5 Cross-section of the GEV3 production well where the measurements took place (credits: CFG).

## 10.5 Data processing

The data processing is based on the PROCATS processing software developed at BRGM (Bourgeois and Girard, 2010). Transfer functions between the magnetic signal at the borehole bottom, at the surface, and the source are calculated for the different emission frequencies. These transfer functions consist of a real part and an imaginary part, corresponding to the in-phase and quadrature components of the subsurface response resulting from the current injection.

The processing involves extracting, for each station, each transmitter polarization, and each injection frequency, the spectral content of the signals recorded at the stations and normalizing them by the dipole moment emitted at the source (the product of the dipole length and the injected current intensity). The result is a measured magnetic induction field in nT/(A·m). This processing allows the magnetic field measured along the borehole axis (or in three spatial directions for the surface station) to be obtained, along with an estimate of the noise for each component. To provide a reference and compare the surface signal with the borehole signal, a magnetic field measurement station was also installed at the wellhead on the boiler plant site. Figure 10.6 shows the respective positions of the source and the receivers

**Table 10.1** *Sampling depths for the magnetic field recording.*

Measurement point	Depth below the end of casing in m
1	105
2	85
3	65
4	55
5	45
6	20
7	-10 (test inside the casing)

**Table 10.2** *Injection sequences.*

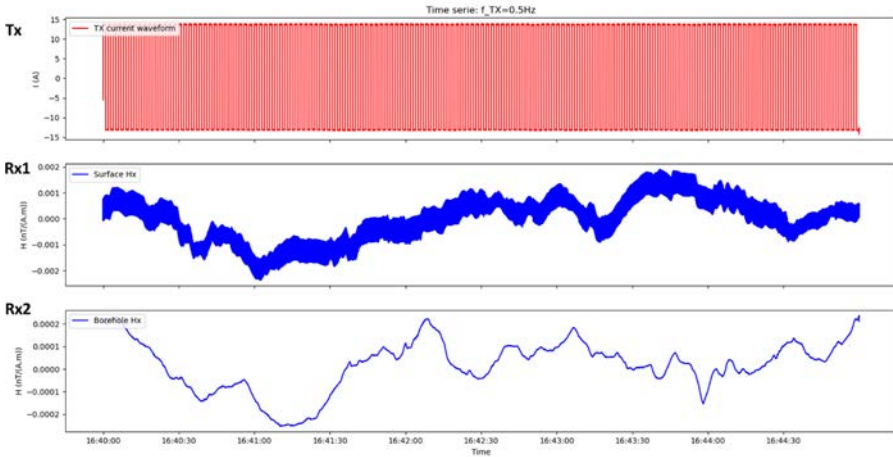
Emitted frequency (Hz)	Duration
0.5	5 min
2	2 min
8	30 s
16	30 s
24	30 s
32	30 s
64	30 s
128	30 s

Figure 10.7 displays the calibrated time series of the signal emitted by the transmitter (TX), the signal received by the surface sensor (RX1), and the signal received by the borehole sensor (RX2). It is clear that the signal emitted by the transmitter is a square wave. A very similar low-frequency behavior is observed between RX1 and RX2. However, the borehole sensor (RX2) shows a significant reduction in high-frequency noise caused by anthropogenic activities. This effect is widely expected as the ground acts as a low-pass filter, removing the high-frequency content from the electromagnetic signal.



Figure 10.6 Positioning map of the source dipole in Sénart Forest (TX2 or TX), the borehole probe at the bottom (RX2), and the surface MT station (RX1).

Figure 10.8 shows the amplitude spectrum of the three time series presented in Figure 10.7. In this example, the signal emitted by the transmitter is a square wave at 0.5 Hz, which appears clearly in the amplitude spectrum's magnitude along with its odd harmonics (1.5, 2.5, 3.5, ...) Hz. Thanks to the noise reduction induced by the ground, the emission peaks from the TX are visible in the borehole magnetometer data (RX2), whereas they are not visible in the surface magnetometer data (RX1). The first clearly visible peak is at 1.5 Hz, which is very distinct on RX2 but completely absent on RX1. These observations clearly show that the signal recorded by the probe corresponds to the signal emitted by the source. The advantage of recording at the borehole bottom to eliminate anthropogenic noise is well validated here. The remaining task is to confirm the order of magnitude of the measured magnetic field value by comparing it with numerical modeling.



**Figure 10.7** Time series of the current emitted by the source (TX), the signal recorded by the surface sensor (RX1), and the signal recorded at the borehole bottom (RX2).

To validate the measurement taken at the borehole bottom, we use a 1D subsurface model, with depth-dependent resistivity variations described in Figure 10.9. We employ the EM3DS software developed by the University of Utah (Wannamaker et al., 1984) to simulate the signal recorded by the probe at the borehole bottom. This software uses a volume integral equation formulation (solved using the method of moments) to compute secondary currents in 3D bounded heterogeneities localized within a 1D stratified structure (infinite horizontal, homogeneous, and isotropic layers). The effect of the casing present in the borehole is not modeled in our case. The signal frequency used for modeling is 0.5 Hz.

The spatial discretization is limited to 3D bodies, while the response of the horizontal stratification is calculated semi-analytically using Hankel transforms. Thanks to this approach, the number of cells in the models remains moderate, generally fewer than 1000 (compared to the typical values of around 100000 in finite-difference or finite-element methods, where the entire 3D space must be meshed), enabling relatively fast computation. The results of this modeling provide a theoretical response at 0.5 Hz of  $7.4 \times 10^{-3}$  nT/(A.m), compared to the recorded signal of  $1.3 \times 10^{-3}$  nT/(A.m). The orders of magnitude are similar, further validating the recorded signal. The observed differences between the modeling and the recorded signal are attributed to the imperfections of the 1D model and the fact that the probe is within the casing.

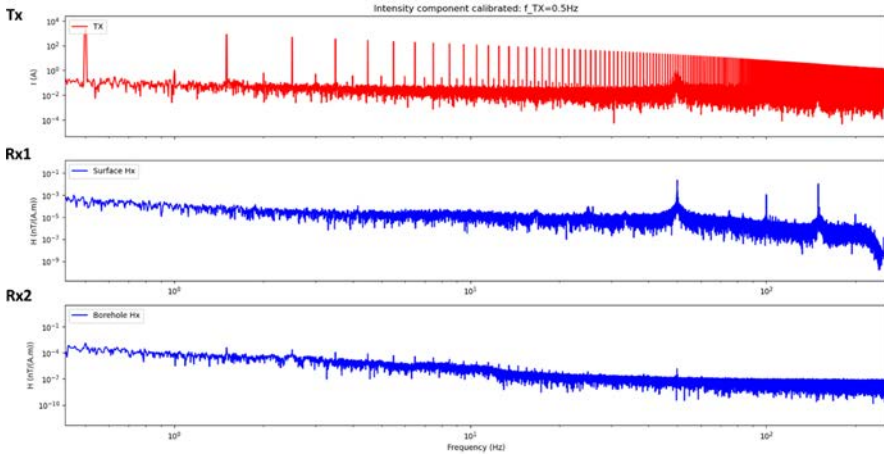


Figure 10.8 Amplitude spectrum of the signal emitted by the source (TX), the signal recorded by the surface receiver (RX1), and the signal recorded at the borehole bottom (RX2).

<b>Top of the layer (m)</b>	0	600	700	1 300	1 400	1 600	1 700	2 000	2 800	3 500
<b>Resistivity (Ω.m)</b>	40	10	40	10	100	1	40	5	20	20

Figure 10.9 Simplified geological model for measurement validation.

## 10.6 Detectability of the cold front

To determine if the cold front is detectable, a new modeling is performed. A parallelepiped with dimensions 100×100×100 m (representing a volume of 10<sup>6</sup> m<sup>3</sup>) simulating water at 40 °C is inserted at the reservoir level. The resistivity of the cold front is chosen to be 41% higher than that of the reservoir layer (based on the experimental tests), which is at 70 °C. Three measurement configurations are modeled (see Figure 10.10) to evaluate the detectability of the cold front. These configurations represent different scenarios we might encounter.

The modeling results are summarized in Figure 10.11. In configuration 1, the magnitude of the secondary field produced by the anomaly (10<sup>-6</sup> nT) is two orders of magnitude higher than the ambient noise level (10<sup>-8</sup> nT). This signal-to-noise ratio

confirms that the cold front could be detected in this configuration, which is a major result of this study. In the other two configurations, 2 and 3, the recorded signal is too weak to allow detection. In configuration 2, the receiver is too far from the source ( $>5$  km), and the response is of the same order of magnitude ( $10^{-8}$  nT) as the noise. In configuration 3, the cold front is too far from the receiver, and the secondary field generated and measured at the receiver is too weak ( $10^{-12}$  nT), well below the noise level, making it undetectable. The main result of this analysis is that in the configuration where the receiver is closest to the anomaly and the source-receiver distance is approximately 3 to 4 km, the anomaly caused by the cold front is detectable.

## Conclusions

The objective of this project was to establish an initial geo-electric state of a geothermal doublet and determine whether a cold front could be detected under ambient noise conditions and using the CSEM sources employed. These objectives were partially achieved. Indeed, the detectability of the cold front was established thanks to the short signal recorded inside the casing. Using the experimental calibrations, which calibrated the variation of resistivity as a function of temperature, the medium's response with and without the cold front was calculated and compared to the noise level extracted from the downhole recordings made by the probe. The modeling shows that the bubble can be detected in specific RX-TX configurations. It was confirmed that the receiver must be as close as possible to the cold front, and the source (transmitter) must be within 4 km of both the bubble and the receiver. These results validate the project's central idea: that a cold front can be detected using the CSEM method (surface-to-well).

During the project's execution, we observed the complexity of installing current sources in a highly urbanized environment. We were fortunate to have the proximity of the Sénart forest to set up the sources and test the method. For this project, we used only one injection site, which would not suffice for imaging purposes. In such cases, several sites at different azimuths would be necessary to accurately locate the cold front in space. During the campaign preparation, six injection sites were identified; however, only three were deemed viable. The others were too close to power lines, pipelines, or in areas where the safety of personnel and equipment could not be ensured. Injection poles require large spaces and the absence of conductive structures (high-voltage lines, pipes, etc.). Therefore, the applicability of the method seems limited to areas with sufficient nearby space to install sources/transmitters unless research efforts can reduce the footprint of these sources.

The receiver may be another project's weak point. It is clear that to further develop this method, work on the probe will be necessary, either internally or through a partnership with specialized manufacturers. For example, integrating three components instead of one could improve result quality. If the above issues are addressed, the most critical challenge remains: access to the well. Obtaining permission to lower

the probe into the GEV3 well was very complicated. The risk of the probe getting stuck is omnipresent, making insurance and risk assessment crucial. Ideally, the measurement should be conducted in the uncased section of the well. There are two main challenges to overcome for this:

1. Obtain authorization to access this zone of the well, where logging tools face a higher risk of getting stuck.
2. Have the physical ability to enter this zone. During this survey, we could not exceed the cased section during the first attempt. Despite repeated efforts by the operator, the probe could not pass through and became temporarily stuck. As a result, measurements were conducted in the cased section of the well. In this case, we currently lack the capability to properly process the data to extract information about the cold front beyond its detectability.

Instrumental and algorithmic developments will thus be necessary to further this concept. Given the undeniable need to monitor the “cold front” and its associated economic implications, it is important to continue exploring solutions to overcome the barriers identified during this project.

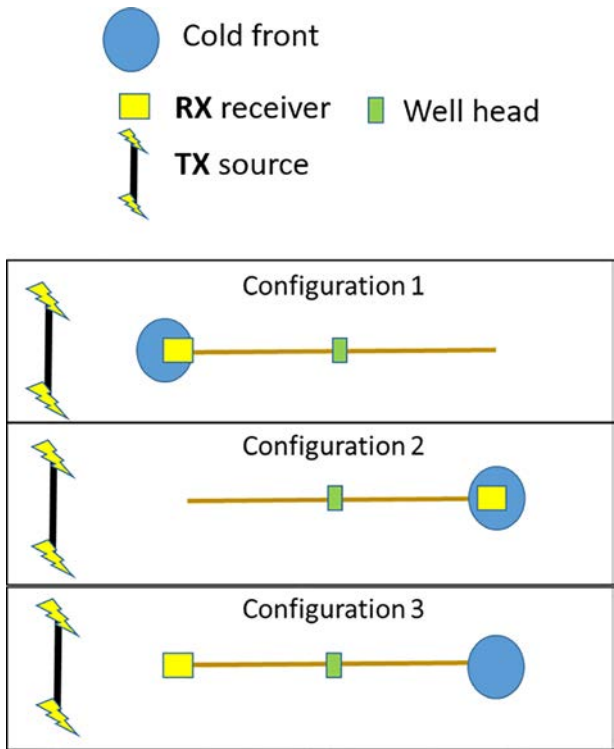


Figure 10.10 Scheme showing the three different geometries between TX-RX modelled to assess the detectability of the cold front.

	configuration 1	configuration 2	configuration 3
<b>Tx</b>	tgt	tgt	tgt
<b>fTx</b>	0,5Hz	0,5Hz	0,5Hz
<b>Rx</b>	puit 1	puit 2	puit 1
<b>Cold front</b>	puit 1	puit 2	puit 2
<b>dRx-Tx</b>	3,5km	5,7 km	3,5km
<b>fRx</b>	<b>0,5Hz</b>	<b>0,5Hz</b>	<b>0,5Hz</b>
<b>Measured signal w/o front nT/A.m</b>	1,3*10 <sup>-3</sup>	??	1,3*10 <sup>-3</sup>
<b>Predicted signal w/o front nT/A.m</b>	7,4*10 <sup>-3</sup>	2,1*10 <sup>-3</sup>	7,4*10 <sup>-3</sup>
<b>fRx</b>	<b>64Hz</b>	<b>64Hz</b>	<b>64Hz</b>
<b>Predicted signal front nT</b>	10 <sup>-6</sup> nT	1,3*10 <sup>-8</sup> nT	10*10 <sup>-12</sup> nT
<b>Noise level (bottom casing nT)</b>	<b>4,7*10<sup>-8</sup>nT</b>	<b>4,7*10<sup>-8</sup>nT</b>	<b>4,7*10<sup>-8</sup>nT</b>
<b>Front detectable?</b>	<b>YES</b>	<b>NO</b>	<b>NO</b>

Figure 10.11 Table summarizing the modeling results and indicating the configurations in which the cold front would be detectable

## References

- Bourgeois B., Girard J.F. (2010) First modelling results of the EM response of a CO2 storage in the Paris Basin, *Oil Gas Sci. Technol.* 65(4), 597-614.
- Revil A., Cathles L.M., Losh S., Nunn J.A. (1998) Electrical conductivity in shaly sands with geophysical applications, *J. Geophys. Res. Solid Earth* 103(10), 23925-23936.
- Wannamaker P.E., SaHohmann G.W., SanFilipo W.A. (1984) Electromagnetic modeling of three-dimensional bodies in layered earths using integral equations, *Geophysics* 149(1), 60-74.
- Wawrzyniak P. (2019) Pilote CO2-Dissolved: Lot 8.1 Monitoring géophysique de la percée thermique par méthode d'Électromagnétisme à Source Contrôlée (CSEM), Rapp. Final BRGM/RP-69370-FR.
- Wawrzyniak P., Coppo N., Bretaudeau F., Vong Chan Q. (2016) CO2-Dissolved: Task 3.2 Geophysical Monitoring, BRGM/RP-66242-FR.